

## Lattice-induced transparency in planar metamaterials

Manukumara Manjappa, Yogesh Kumar Srivastava, and Ranjan Singh\*

*Division of Physics and Applied Physics, School of Physical and Mathematical Sciences, Nanyang Technological University,  
21 Nanyang Link, Singapore 637371, Singapore  
and Center for Disruptive Photonic Technologies, The Photonics Institute, Nanyang Technological University,  
50 Nanyang Avenue, Singapore 639798, Singapore  
(Received 8 May 2016; published 4 October 2016)*

Lattice modes are intrinsic to periodic structures and they can be easily tuned and controlled by changing the lattice constant of the structural array. Previous studies have revealed the excitation of sharp absorption resonances due to lattice mode coupling with the plasmonic resonances. Here, we report an experimental observation of a lattice-induced transparency (LIT) by coupling the first-order lattice mode (FOLM) to the structural resonance of a terahertz asymmetric split ring resonator. The observed sharp transparency is a result of the destructive interference between the bright mode and the FOLM assisted dark mode. As the FOLM is swept across the metamaterial resonance, the transparency band undergoes a large change in its bandwidth and resonance position. We propose a three-oscillator model to explain the underlying coupling mechanism in LIT system that shows good agreement with the observed results. Besides controlling the transparency behavior, LIT also shows a huge enhancement in its  $Q$  factor and exhibits a high group delay of 28 ps with an enhanced group index of  $4.5 \times 10^4$ , which could be pivotal in ultrasensitive sensing and slow-light device applications.

DOI: [10.1103/PhysRevB.94.161103](https://doi.org/10.1103/PhysRevB.94.161103)

Metamaterials (MMs) [1,2] are arguably one of the simplest materials to control and engineer the resonance properties of the light-matter interaction by altering the geometry of their structures. A perfect lens [3,4], negative refraction [5], invisibility cloak [6], phase engineering, and many more intriguing phenomena have been realized by exploiting the impressive properties offered by MMs. In recent years, engineering resonant transmission properties in the terahertz band of the electromagnetic spectrum using MM structures has gained tremendous interest for achieving anomalous behavior in the phase of the propagating field. One way of tailoring the phase anomalies using metamaterials is by inducing a sharp transparency through intra-unit-cell coupling of bright-dark resonances via a Fano-type interference [7–20]. In such a system, achieving a transmission window with a higher quality factor ( $Q$ ) is quite challenging, which is limited by the linewidth of the dark mode. Here, we overcome this limitation by diffraction coupling the metamaterial resonances in an asymmetric split ring resonator structure to induce a transparency peak with enhanced  $Q$  factors. This transparency is mediated and tailored by the lattice mode, which can be adequately controlled by varying the lattice constant of the metamaterial structure, and provides an efficient way to modulate frequency, amplitude, and the linewidth of the transmission resonances.

Lattice mode resonances often appear due to a discontinuity in the dispersion curves at ambient medium-substrate interfaces at the Rayleigh cutoff wavelengths [21,22] of an incident field. These are also referred to as diffractive modes or Wood anomalies [23], whose spectral position depends on the periodicity of the unit cell and the incident angle of the excitation field. The anomalies appearing due to diffraction are intrinsic to subwavelength periodic structures such as

metamaterials and, despite their attractive features, such as extremely narrow resonances and broadband tunability, they have not been much explored. In the past, there have been a handful of works demonstrating the implications of these lattice modes in periodic structures. Coupling the plasmonic/metamaterial resonances to the lattice modes has yielded resonant suppression in the light extinction [24], and extremely high  $Q$  resonances at the near infrared [25–27] and far infrared frequencies [28], but these observations have not shown any signature that alters the nature of the metamaterial resonance itself. In this Rapid Communication, we demonstrate an experimental observation of lattice-induced transparency (LIT) by coupling the first-order lattice mode (FOLM) to the MM structural mode of a periodically arranged terahertz asymmetric split ring resonator (TASR) MM structure.

To investigate the influence of the lattice mode on MM resonances, we considered MM samples consisting of a TASR structure with varying square lattice constants, as shown in Fig. 1. Samples were fabricated using the conventional photolithography technique, where an aluminum metal of thickness,  $T = 200$  nm was deposited on a  $500 \mu\text{m}$  thick high resistivity ( $\rho > 5000$ ) silicon substrate ( $\epsilon_r = 11.7$ ) using the thermal evaporation method followed by a lift-off process. Figure 1(d) shows the unit-cell dimensions of the fabricated TASR MM samples with varying lattice constants (periodicity)  $P = 65, 80, \text{ and } 95 \mu\text{m}$ . The structural dimensions of the depicted samples were kept the same and only the periodicity of the structure along the  $x$  and  $y$  axes was varied to tune the resonance frequency of the lattice mode. The resonance frequency for the lattice mode is determined by the following simplified expression for a periodic square lattice and for a normal beam incidence,

$$f_{\text{diff}} = \frac{c}{nP} \sqrt{i^2 + j^2}, \quad (1)$$

where  $c$  is the speed of light in vacuum,  $n$  is the refractive index of the substrate,  $P$  is the lattice constant of the structure

\*ranjans@ntu.edu.sg

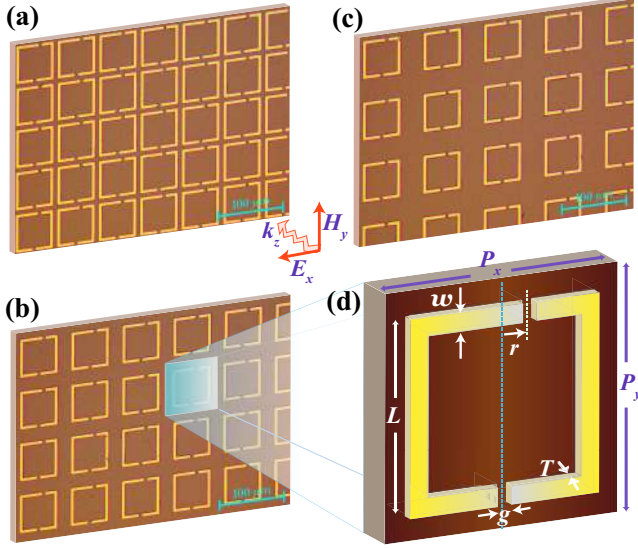


FIG. 1. (a)–(c) are the optical microscopy (OM) images of the metamaterial samples with lattice constant/periodicity  $P_x = P_y = P = 65, 80,$  and  $95 \mu\text{m}$ , respectively. (d) depicts the unit-cell dimensions of the metamaterial sample. Length,  $L$ :  $60 \mu\text{m}$ ; asymmetry,  $r$ :  $8 \mu\text{m}$ ; gap,  $g$ :  $3 \mu\text{m}$ ; width,  $w$ :  $6 \mu\text{m}$ ; and thickness of metal,  $T$ :  $200 \text{ nm}$ .

and  $(i, j)$  are the pair of indices defining the order of the lattice mode. For the first-order lattice mode (FOLM)  $(0, 1)$ , the above expression reduces to  $f_{\text{diff}} = \frac{c}{nP}$ , where the frequency of the lattice mode varies inversely with the lattice constant ( $P$ ).

In this work, we numerically as well as experimentally investigate the effect of FOLM on the dipolar resonance appearing at  $1.1 \text{ THz}$  for the incident polarization  $E_x$ . This investigation was primarily performed by rigorous numerical simulations using the finite integral techniques method offered by the CST Microwave Studio Frequency Solver. It is important to note that in the numerical simulations, where the resonance possesses high  $Q$ -factors, choice of the material plays a critical role [16]. Hence, materials for the numerical simulation were chosen to be an aluminum metal with DC conductivity ( $\sigma_{DC} = 35.6 \text{ MS/m}$ ) as the TASR metallic resonators and silicon with dielectric constant  $\epsilon = 11.7$  used as the transparent substrate at terahertz frequencies. In the simulations, the lattice constant ( $P$ ) for the MM unit cell is chosen in such a way that for  $P = 80 \mu\text{m}$ , the FOLM is precisely matched to the TASR resonance at  $1.1 \text{ THz}$ , whereas for  $P = 65$  and  $95 \mu\text{m}$ , FOLM is towards the blue and the red side of the TASR resonance, respectively. The green curve in Fig. 2(a) depicts the simulated transmission response for the MM sample with a lattice constant  $P = 95 \mu\text{m}$  for the  $E_x$  excitation. We observe a very weak coupling of the metamaterial resonance to the lattice mode (near  $0.9 \text{ THz}$ ) that is hard to detect in the far field. This weak coupling is due to a large offset in the respective resonance frequencies of the metamaterial mode and the lattice mode, and the other reason is due to decreased near field effects from the nearest neighboring unit cells for larger periodicities [29]. The other sharp feature observed around  $1.3 \text{ THz}$  corresponds to the coupling with a higher-order  $(I, I)$  lattice mode.

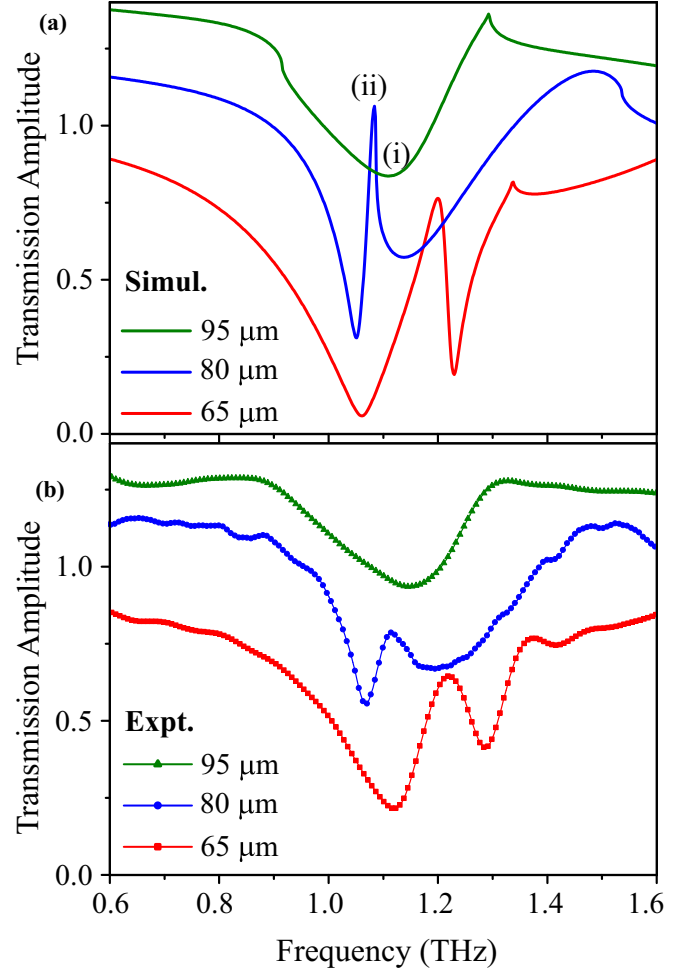


FIG. 2. (a) Numerically simulated curves depicting the modulation of the transmission window for various lattice constants ( $P = 65, 80,$  and  $95 \mu\text{m}$ ) of the metamaterial structure. (b) Experimental curves justifying the numerically predicted results. The curves are drawn with a vertical offset for better visibility.

As the periodicity of the structure is decreased to  $80 \mu\text{m}$ , we notice a strong coupling of the MM eigenresonance to the FOLM, which results in a sharp transparency, as shown by the blue curve in Fig. 2(a). When the  $E_x$  polarized light is incident on the sample, a broad dipolar resonance centered at  $1.1 \text{ THz}$  interacts resonantly with weakly oscillating FOLM that propagates on the surface of the substrate. The first-order lattice mode whose energy gets trapped within the MM array couples to the other surface modes rather than to the free space and mediates the excitation of the otherwise unexcited dark mode (results due to structural asymmetry) within the TASR MM system. This interaction between the broad MM resonance mode and the weakly excited dark mode that is mediated by the lattice mode undergoes a Fano-type interference to give rise to a sharp transmission window. As the lattice constant is decreased to  $65 \mu\text{m}$ , the FOLM is blueshifted with respect to the MM resonance, which results in a blueshift of the observed transmission peak, as shown by the red curve in Fig. 2(a). The increased linewidth and the strength of the transmission resonance for  $P = 65 \mu\text{m}$  is mainly due to the increased near field interactions of the

neighboring unit cells for smaller periodicities. Here, it is worth mentioning that the LIT effect is purely from the coupling of the resonances within the unit cell (intra-unit-cell coupling). If the coupling contribution is from the intra-unit-cell alone, we should observe a weak transmission window showing the similar strengths at the lower and the higher frequency part of the spectrum. However, it is not the case in the numerical simulations and the experiment, where we observe additional coupling effects from the inter-unit-cell coupling of the nearest neighboring unit cells. Hence, we see a very weak excitation of a transmission window near 0.9 THz for  $P = 95 \mu\text{m}$ , where the inter-unit-cell coupling is weak and a strong transmission window with a broader linewidth for  $P = 65 \mu\text{m}$  is due to strong inter-unit-cell coupling of the neighboring unit cells. We emphasize that such an asymmetric nature of coupling can be eliminated by sweeping the resonance frequency of MM across the FOLM by keeping the lattice constants fixed, thus not altering the inter-unit-cell coupling in the system. Figure 2(b) displays the experimental results measured using the standard photoconductive antenna based THz-time domain spectroscopy (THz-TDS) setup, where the transmission response of the metamaterial sample  $[E_S(\omega)]$  is normalized to the reference substrate transmission  $[E_R(\omega)]$  using the relation  $|T(\omega)| = |\frac{E_S(\omega)}{E_R(\omega)}|$ . The measured transmission response shows good agreement with the numerical simulations, except for  $P = 80 \mu\text{m}$  where the sharp transmission peak seen in the simulation is not captured in the experiments due to the resolution limitations of our THz-TDS setup.

To theoretically investigate the coupling behavior responsible for the LIT phenomenon, we propose a three-oscillator model, wherein two dark modes (lattice and the asymmetric modes), which are weakly coupled to the free space field, interact with a bright mode (metamaterial mode that is strongly excited by the incident field) to result in an enhanced sharp transmission window, instead of inducing multiple transparency peaks as observed in Refs. [30–32]. We write the equations of motion for the three coupled oscillators, namely, the bright mode, lattice mode, and the dark mode in the frequency domain, respectively, as follows:

$$(-\omega^2 - i\omega\gamma_b + \omega_b^2)\tilde{x}_b + \Omega_1^2\tilde{x}_{\text{LM}} = \tilde{E}(\omega), \quad (2)$$

$$(-\omega^2 - i\omega\gamma_{\text{LM}} + \omega_{\text{LM}}^2)\tilde{x}_{\text{LM}} + \Omega_1^2\tilde{x}_b - \Omega_2^2\tilde{x}_d = 0, \quad (3)$$

$$(-\omega^2 - i\omega\gamma_d + \omega_d^2)\tilde{x}_d + \Omega_2^2\tilde{x}_{\text{LM}} = 0. \quad (4)$$

The terms  $(\omega_b, \omega_{\text{LM}}, \omega_d)$  and  $(\gamma_b, \gamma_{\text{LM}}, \gamma_d)$  represent the resonance and the damping frequencies of the bright mode (metamaterial eigenmode), lattice mode, and the dark (asymmetric) mode, respectively.  $\Omega_1$  and  $\Omega_2$  are the coupling strengths between the bright-lattice modes and the lattice-dark modes, respectively (shown in the inset schematic of Fig. 3). It is worth noting that the coupling of the bright mode to the dark (asymmetry) mode is mediated by the lattice mode as described by the above coupled expressions [Eqs. (1)–(3)]. Hence, for  $\omega_d = \omega_{\text{LM}}$  and  $\gamma_d = \gamma_{\text{LM}}$ , we arrive at the analytic expression for the scattering amplitude for the bright eigenmode, which is given by

$$\tilde{x}_b = \frac{-E[\Omega_2^4 + (\omega^2 - \omega_{\text{LM}}^2 + i\omega\gamma_{\text{LM}})^2]}{[(\Omega_2^4 + (\omega^2 - \omega_{\text{LM}}^2 + i\omega\gamma_{\text{LM}})^2)(\omega^2 - \omega_b^2 + i\omega\gamma_b)] - \Omega_1^4(\omega^2 - \omega_{\text{LM}}^2 + i\omega\gamma_{\text{LM}})}. \quad (5)$$

Using expression (5), we plot the transmission spectrum  $(1 - \text{Im}[\tilde{x}_b])$  by varying the resonance frequency of the lattice mode ( $\omega_{\text{LM}}$ ) for the following set of realistic system parameters,  $\Omega_1 = \Omega_2 = 1$ ,  $\omega_b = 6.9$ ,  $\gamma_b = 1$ ,  $\gamma_{\text{LM}} = 0.15$ , and  $E = 0.17$ , and the results are shown in Fig. 3. It is worth mentioning that the proposed theoretical model [Eq. (5)] does not take account of the near field influence due to inter-unit-cell coupling for varied periodicity. Hence, there are small discrepancies observed in the linewidths of the theoretical curves compared with the simulated/experimental results for the periodicities  $P = 65, 80$ , and  $95 \mu\text{m}$ , but otherwise they show a good agreement.

The underlying near field effects in the LIT are further understood by studying the surface current distribution at the resonance dip (i) for  $P = 95 \mu\text{m}$  and at the transparency peak (ii) for  $P = 80 \mu\text{m}$ , as shown in Fig. 4. The MM eigenresonance that is not matched to the FOLM (for  $P = 95 \mu\text{m}$ ) results in a dipolar type of surface current, where the currents on the resonator arms run parallel to the electric component of the excitation field  $E_x$ . When the MM dipolar resonance is matched to the FOLM (for  $P = 80 \mu\text{m}$ ), the energy propagated on the surface of the substrate interacts with the MM dipole resonance to induce antiparallel currents

along the opposite arms of the resonator. These opposing currents are quadrupolar in nature and destructively interfere to result in the cancellation of the fields at the resonance, leading to a sharp transmission peak and steep dispersion within the system. Thus the nature of MM resonance is modified by the influence of the lattice mode, which alters the dipolar type of resonance into a sharp transmission feature showing the quadrupolar nature of the surface currents.

Figure 5 represents the contour diagram showing the intensity variation of the transmitted field with respect to the frequency of the incident beam and the lattice constants of the MM structure. Variation in the frequency of the FOLM with respect to the lattice constant is also plotted and is shown by the red dashed-dotted lines in Fig. 5. As observed, a shift in the frequency of the transparency peak follows the frequency shift of the FOLM. As the FOLM approaches the TARS MM resonance, we observe a gradual narrowing of the resulting transmission peak. This enhanced sharpness in the transmission window can be attributed to increased diffraction effects near the resonance that traps the energy in the MM array and suppresses the radiation propagating into the far field. The extracted  $Q$  factors of the LIT band from the

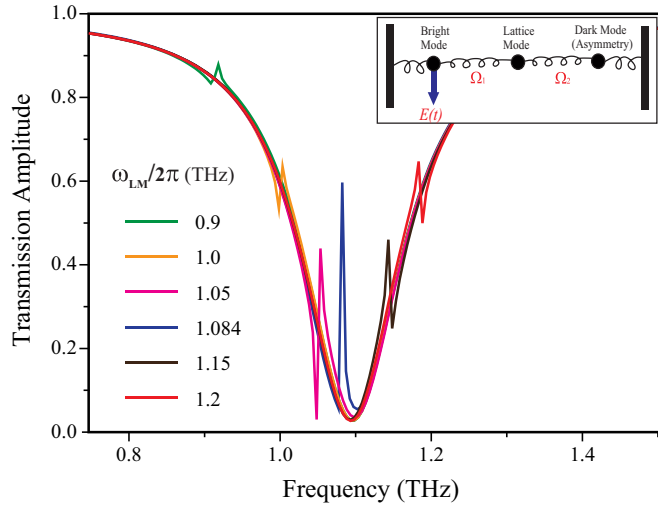


FIG. 3. Transmission resonances extracted from the three-oscillator model [Eq. (5)] for varying resonance frequencies of the lattice mode ( $\omega_{LM}$ ). The lattice mode frequencies  $\frac{\omega_{LM}}{2\pi} = 0.9, 1.084,$  and  $1.2$  THz correspond to the lattice periodicities  $P = 95, 80,$  and  $65 \mu\text{m}$  of Fig. 2, respectively. The inset figure represents the schematic of the bright-dark-dark coupling in the LIT system.

simulated transmission curves are 25, 30, 35, and 91 for  $P = 65, 70, 75,$  and  $80 \mu\text{m}$ , respectively. For the observed transparency peaks, we extract the figure of merit (FOM), which quantifies the strength of the resonance in terms of product of the  $Q$  factor and intensity of the transparency peak ( $\text{FOM} = Q \times \Delta I$ ). The defined FOM is an optimized parameter for realizing efficient devices for ultrasensitive [33] and nonlinear applications. FOMs for the transparency peak for the lattice constants  $P = 65, 70, 75,$  and  $80 \mu\text{m}$  are 13.7, 18.4, 23.6, and 55, respectively. For  $P = 80 \mu\text{m}$ , where the FOLM is exactly matched to the resonance of the TASR mode, we observe a steep rise in the  $Q$  factor (91) and FOM (55) for the transparency that is higher than the previous value observed for these structures at THz frequencies [34]. Since the observed LIT effect is scalable, it opens up an avenue for achieving a high  $Q$  transparency behavior at higher frequencies by compensating material losses in the system.

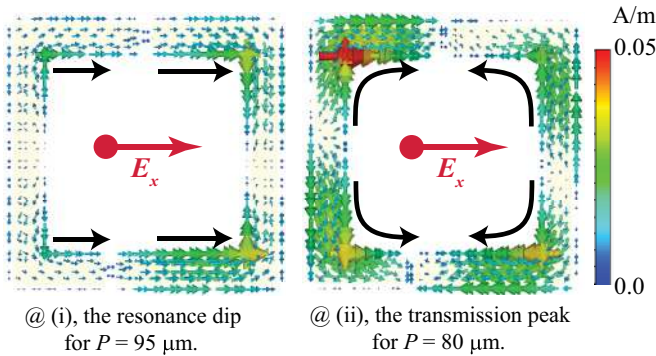


FIG. 4. Simulated surface current distribution at resonance dip (i) for  $P = 95 \mu\text{m}$  and at the transparency peak (ii) for  $P = 80 \mu\text{m}$  for the curves shown in Fig. 2(a).

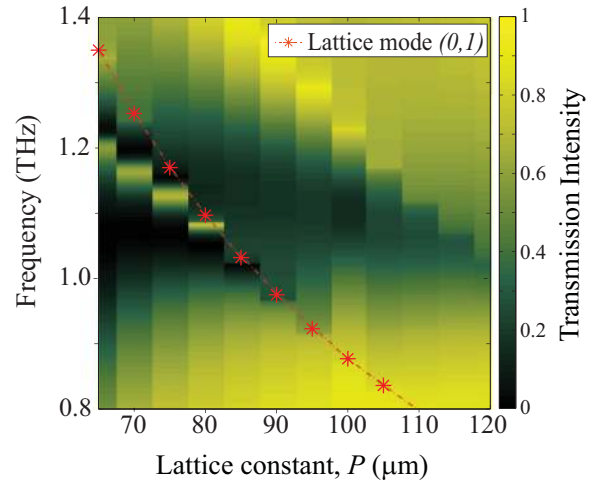


FIG. 5. Contour plot showing the variation in the transmission intensity of the LIT resonance as a function of frequency vs the lattice constant. The red dashed-dotted curve signifies the resonance variation of the first-order lattice mode (FOLM) ( $0,1$ ) with varying lattice constants ( $P$ ). There is a clear indication that the change in the position of the transparency peak follows the variation of FOLM.

Improved sharpness in the transparency peak observed due to diffraction coupling induces an anomalous resonant dispersion that enhances the slow-light behavior within the system. The slow-light nature of the pulse is quantified in terms of the group delay values extracted from the phase of the pulse propagating through the medium by using the expression  $t_g = -\frac{d\phi}{d\omega}$ , where  $\phi$  is the phase delay in the pulse propagating through the medium and  $\omega$  is the angular frequency of the incident pulse. As illustrated in Fig. 6, our simulation results estimate as high as 28 ps of delay in the group velocity of the terahertz pulse through the MM sample with the lattice constant  $P = 80 \mu\text{m}$ , whereas for  $P = 65 \mu\text{m}$  the group delay is around 10 ps. A sharp increase in the group delay value for  $P = 80 \mu\text{m}$  is attributed to the strong interaction of the MM resonance with the FOLM, which slows down the propagation of light quite drastically. Coupling

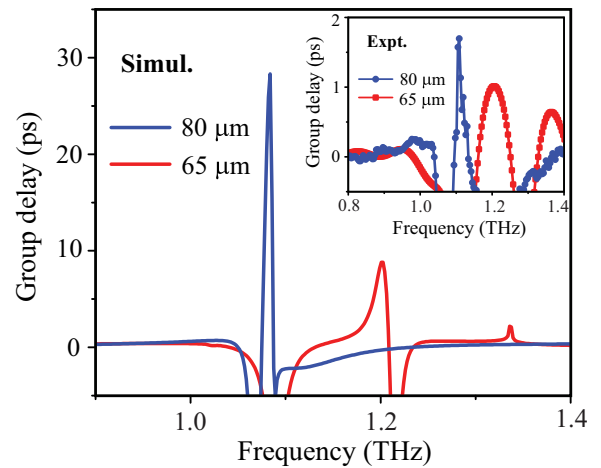


FIG. 6. Numerically obtained group delay plots for lattice constants  $P = 65$  and  $80 \mu\text{m}$ . The inset figure represents the group delay curve extracted from the measured data.

the metamaterial resonances with the nearby lattice mode gives a great advantage of tailoring the group delay in the incident terahertz pulse with a remarkable enhancement in the slow-light behavior within the system. The group delay values shown in the inset of Fig. 6 are extracted from the measured data and show similar trends as observed in the simulations. The group index for the LIT sample with  $P = 80 \mu\text{m}$  can reach very large values, as high as  $4.5 \times 10^4$  at 1.084 THz and  $1.5 \times 10^4$  at 1.2 THz for the sample with  $P = 65 \mu\text{m}$ . The group index values are calculated by using the formula  $n_g = \frac{c}{v_g} = \frac{ct_g}{T}$ , where  $T$  is the thickness of the metal resonator,  $t_g$  is the group delay, and  $c$  is the speed of light. Recently, we became aware of a study that reported an enhanced group delay of up to 25 ps and a 4 order of magnitude increase in the group index in a diffraction-enhanced transparency system at terahertz frequencies [35]. Although their work reports enhanced resonance properties as observed in our proposed LIT system, the mechanisms involved are different. The surface lattice mode in the LIT system takes part in inducing the transparency peak as well as in enhancing its sharpness, whereas in Ref. [35] the surface lattice modes are coupled to an already existing transmission window to enhance its strength.

In conclusion, we have demonstrated lattice-induced transparency (LIT) in a planar metamaterial by radiatively coupling the metamaterial resonances with the first-order lattice mode (FOLM). The nature of the LIT transmission band was modulated by sweeping the lattice mode across the metamaterial eigenresonance by changing the periodicity of the metamaterial sample. Our results demonstrate a very sharp transmission feature with a significantly enhanced group delay for the incident terahertz pulse. Moreover, our study provides insights into realizing sharp transparency resonances by coupling the superradiant (bright) mode to multiple subradiant (dark) modes, which can enhance their  $Q$  factors by several times, and which can be exploited in ultrasensitive sensors and nonlinear applications. These lattice coupled systems can be of great interest in many real world applications, such as in fast growing broadband communication technologies as optical routers and phase retarders, and slow-light devices.

We would like to acknowledge the research funding support from NTU startup Grant No. M4081282, Singapore MOE Grants No. M4011362, No. M4011534, No. MOE2011-T3-1-005, and No. MOE2015-T2-2-103.

- 
- [1] J. B. Pendry, A. J. Holden, D. J. Robbins, and W. J. Stewart, *IEEE Trans. Microwave Theory Tech.* **47**, 2075 (1999).
- [2] D. R. Smith, W. J. Padilla, D. C. Vier, S. C. Nemat-Nasser, and S. Schultz, *Phys. Rev. Lett.* **84**, 4184 (2000).
- [3] J. B. Pendry, *Phys. Rev. Lett.* **85**, 3966 (2000).
- [4] N. Fang, H. Lee, C. Sun, and X. Zhang, *Science* **308**, 534 (2005).
- [5] D. R. Smith, J. B. Pendry, and M. C. K. Wiltshire, *Science* **305**, 788 (2005).
- [6] D. Schurig, J. J. Mock, B. J. Justice, S. A. Cummer, J. B. Pendry, A. F. Starr, and D. R. Smith, *Science* **314**, 977 (2006).
- [7] S. Zhang, D. A. Genov, Y. Wang, M. Liu, and X. Zhang, *Phys. Rev. Lett.* **101**, 047401 (2008).
- [8] N. Papasimakis, V. A. Fedotov, N. I. Zheludev, and S. L. Prosvirnin, *Phys. Rev. Lett.* **101**, 253903 (2008).
- [9] R. Singh, C. Rockstuhl, F. Lederer, and W. Zhang, *Phys. Rev. B* **79**, 085111 (2009).
- [10] N. Liu, L. Langguth, T. Weiss, J. Kastel, M. Fleischhauer, T. Pfau, and H. Giessen, *Nat. Mater.* **8**, 758 (2009).
- [11] J. Gu, R. Singh, X. Liu, X. Zhang, Y. Ma, S. Zhang, S. A. Maier, Z. Tian, A. K. Azad, H.-T. Chen, A. J. Taylor, J. Han, and W. Zhang, *Nat. Commun.* **3**, 1151 (2012).
- [12] Y. Yang, I. I. Kravchenko, D. P. Briggs, and J. Valentine, *Nat. Commun.* **5**, 5753 (2014).
- [13] M. Manjappa, S.-Y. Chiam, L. Cong, A. A. Bettiol, W. Zhang, and R. Singh, *Appl. Phys. Lett.* **106**, 181101 (2015).
- [14] R. Singh, I. Al-Naib, Y. Yang, D. R. Chowdhury, W. Cao, C. Rockstuhl, T. Ozaki, R. Morandotti, and W. Zhang, *Appl. Phys. Lett.* **99**, 201107 (2011).
- [15] P. Pitchappa, M. Manjappa, C.P. Ho, R. Singh, N. Singh, and C. Lee, *Adv. Opt. Mater.* **4**, 541 (2016).
- [16] Y. K. Srivastava, M. Manjappa, L. Cong, W. Cao, I. Al-Naib, W. Zhang, and R. Singh, *Adv. Opt. Mater.* **4**, 457 (2016).
- [17] R. Singh, I. Al-Naib, W. Cao, C. Rockstuhl, M. Koch, and W. Zhang, *IEEE Transactions on Terahertz Science and Technology* **3**, 820 (2013).
- [18] G. Dayal, X. Y. Chin, C. Soci, and R. Singh, *Adv. Opt. Mater.* **4**, 1295 (2016).
- [19] L. Cong, M. Manjappa, N. Xu, I. Al Naib, W. Zhang, and R. Singh, *Adv. Opt. Mater.* **3**, 1537 (2015).
- [20] Y. K. Srivastava, M. Manjappa, H. N. S. Krishnamoorthy, and R. Singh, *Adv. Opt. Mater.*, DOI: 10.1002/adom.201600354.
- [21] L. Rayleigh, *Proc. R. Soc. London, Ser. A* **79**, 399 (1907).
- [22] V. G. Kravets, F. Schedin, and A. N. Grigorenko, *Phys. Rev. Lett.* **101**, 087403 (2008).
- [23] R. W. Wood, *Philos. Mag.* **4**, 396 (1902).
- [24] S. Linden, J. Kuhl, and H. Giessen, *Phys. Rev. Lett.* **86**, 4688 (2001).
- [25] E. M. Hicks, S. Zou, G. C. Schatz, K. G. Spears, R. P. Van Duyne, L. Gunnarsson, T. Rindzevicius, B. Kasemo, and M. Käll, *Nano Lett.* **5**, 1065 (2005).
- [26] B. Auguie and W. L. Barnes, *Phys. Rev. Lett.* **101**, 143902 (2008).
- [27] J. Sung, E. M. Hicks, R. P. Van Duyne, and K. G. Spears, *J. Phys. Chem. C* **112**, 4091 (2008).
- [28] A. Bitzer, J. Wallauer, H. Helm, H. Merbold, T. Feurer, and M. Walther, *Opt. Express* **17**, 22108 (2009).
- [29] N. Xu, R. Singh, and W. Zhang, *J. Appl. Phys.* **118**, 163102 (2015).
- [30] H. Xu, Y. Lu, Y.-P. Lee, and B. S. Ham, *Opt. Express* **18**, 17736 (2010).
- [31] P. K. Jha, M. Mrejen, J. Kim, C. Wu, X. Yin, Y. Wang, and X. Zhang, *Appl. Phys. Lett.* **105**, 111109 (2014).

- [32] N. Xu, M. Manjappa, R. Singh, and W. Zhang, *Adv. Opt. Mater.* **4**, 1179 (2016).
- [33] L. Cong, S. Tan, R. Yahiaoui, F. Yan, W. Zhang, and R. Singh, *Appl. Phys. Lett.* **106**, 031107 (2015).
- [34] W. Cao, R. Singh, I. A. I Al-Naib, M. He, A. J. Taylor, and W. Zhang, *Opt. Lett.* **37**, 3366 (2012).
- [35] M. C. Schaafsma, A. Bhattacharya, and J. Gómez Rivas, *ACS Photonics* **3**, 1596 (2016).